UC Irvine
UC Irvine Previously Published Works

Title
Quantitative analysis of peri-tumor fat in different molecular subtypes of breast cancer

Permalink
https://escholarship.org/uc/item/5rt9f29s

Authors
Chen, Jeon-Hor
Zhang, Yang
Chan, Siwa
et al.

Publication Date
2018-11-01

DOI
10.1016/j.mri.2018.06.019

Peer reviewed

eScholarship.org Powered by the California Digital Library
University of California

Author Manuscript

Author Manuscript

Author Manuscript

Author Manuscript

HHS Public Access

Author manuscript

Magn Reson Imaging. Author manuscript; available in PMC 2019 November 01.

Published in final edited form as:

Magn Reson Imaging. 2018 November ; 53: 34–39. doi:10.1016/j.mri.2018.06.019.

Quantitative analysis of peri-tumor fat in different molecular subtypes of breast cancer

Jeon-Hor Chen[a,b,*], **Yang Zhang**[a], **Siwa Chan**[c,d,e], **Ruey-Feng Chang**[c], **Min-Ying Su**[a]

[a]Center For Functional Onco-Imaging of Department of Radiological Sciences, University of California, Irvine, CA, USA

[b]Department of Radiology, E-Da Hospital and I-Shou University, Kaohsiung, Taiwan

[c]Graduate Institute of Biomedical Electronics and Bioinformatics, National Taiwan University, Taipei, Taiwan

[d]Department of Medical Imaging, Taichung Tzu Chi Hospital, Buddhist Tzu Chi Medical Foundation, Taichung, Taiwan

[e]Department of Radiology, School of Medicine, Tzu Chi University, Hualien, Taiwan

Abstract

Background and purposes: The aim of this study was to develop morphological analytic methods to analyze the tumor-fat interface and in different peritumoral shells away from the tumor, and to compare the results among three molecular subtypes of breast cancer.

Materials and methods: A total of 102 women (mean age 48.5 y/o) with solitary well-defined breast cancers were analyzed, including 46 human epidermal growth factor receptor 2 (HER2) (+), 46 HER2(−) hormonal receptor (HR) (+), and 10 triple negative (TN) breast cancers. The tumor lesion, the breast, the fibroglandular and fatty tissue were segmented using well-established methods. The whole breast fat percentage and the peri-tumor interface fat percentage were measured. Three shells (SH1, SH2, SH3) surrounding the convex hall of the three dimensional (3D) tumor were defined and in each shell the volumetric percentage of fat was calculated. The peri-tumor interface fat percentage and the volumetric percentage of fat in the three peri-tumoral shells were compared among different subtypes.

Results: In the TN group, the fat percentage on the tumor boundary was 43 ± 20% and 78 ± 12% for two dimensional (2D) and 3D measurement, respectively, which were the highest among the three subtypes but not significantly different. The fat percentage in SH2 and SH3 in the TN group was 82 ± 7% and 85 ± 7%, which was significantly higher compared to the two other two subtypes. The results remained after controlling for the whole breast fat percentage.

Conclusions: This study provided a feasible method for quantitative analysis of peri-tumoral tissue characteristics. Because of small patient number, the finding that TN tumors had the highest peri-tumor fat content among the three subtypes needs to be further verified with a large cohort study.

*Corresponding author at: John Tu and Thomas Yuen Center for Functional Onco-Imaging, 164 Irvine Hall, University of California, Irvine, CA 92697-5020, USA. jeonhc@uci.edu (J.-H. Chen).

Author Manuscript Author Manuscript Author Manuscript Author Manuscript

1. Introduction

The peritumoral region, the area surrounding the tumor, may possess valuable information. Peritumoral tissue may be different from the normal tissue due to tumor invasion [1, 2], tissue reactions [3], and tissue changes [4, 5]. The breast is composed of two predominant tissue types, the fibroglandular tissue and the adipose tissue [6]. Although breast carcinoma arises from the epithelial cells that line the lobules and terminal ducts of breast glandular tissue, many epidemiological studies have shown that excessive body adipose tissue is a risk factor for several cancer types, including breast cancer, and can also lead to poorer treatment outcome [7]. It has been shown that peritumoral adipose tissue and secreted steroids and adipokine contribute to the occurrence of breast cancer [8]. The adipose tissue that is abundantly present around the ductal epithelium of the mammary gland may function as a slow-release depot for lipid-soluble carcinogenic agents, and thus may affect cancer risk [9].

Studies have also shown that fat tissue close to malignant and benign lesions exhibited distinctive gene expression profiles and functional characteristics [10]. Fatty acid fractions in breast adipose tissue were also different in malignant and benign breast tumor [11]. A recent study using magnetic resonance imaging (MRI) showed invasive breast cancer preferably and predominantly occurs adjacent to breast adipose tissue [12]. Another study also found that malignant lesions were located in or near the interface in significantly higher proportions than benign lesions [13]. The tumor-surrounding adipose tissue was also reported as a key component of breast cancer progression [14, 15]. In women with early stage breast cancer, peritumoral fat correlates positively with the ratio of pathologically involved axillary nodes [14]. Imaging studies of breast peritumoral tissue have been performed to predict treatment response [16] and lymphovascular invasion [17], and to correlate with pathological biomarkers [18].

The purpose of this study is to use MR imaging to evaluate the peritumoral adipose tissue quantitatively. The interface of the tumor adjacent to fat vs. fibroglandular tissue, and the percentage of fat volume in the peritumoral shells at different distances from the tumor periphery were measured. Molecular biomarkers including HER2, estrogen receptor (ER), progesterone receptor (PR), or combined Hormonal receptor (HR) were used to differentiate breast cancer subtypes. Since different subtypes have different tumor morphology and aggressiveness, the measured peritumoral fat results in three subtypes: HER2(+), HER2(−)HR(+), and HER2(−)HR(−) (i.e. triple negative TN) were reported and compared.

2. Materials and methods

2.1. Patients

This was a retrospective study approved by our Institutional Review Board and the informed consent was waived. From August 2013 to December 2014, 102 women (range 22–75, mean age 48.5 y/o) with pathologically proven solitary well-defined breast cancer (tumor size 0.4–5.0 cm, mean 2.6 cm) were studied. These were clinical patients receiving MRI for diagnosis or pre-operative staging. Most patients ($N = 97$) had invasive cancer and 5 patients had ductal carcinoma in situ (DCIS). For cancer subtypes, 46 patients had HER2 positive, 46 had HER2 negative HR positive, and 10 patients had triple negative (TN) cancer.

Author Manuscript Author Manuscript Author Manuscript Author Manuscript

2.2. MR imaging

All MR examinations were done by using a 1.5-Tesla scanner (Magneton Skyra, Siemens Medical Solutions, Erlangen, Germany), with a 16-channel Sentinelle breast coil. DCE-MRI was acquired by using the fat-suppressed 3D-FLASH with one pre-contrast and four post-contrast frames, with TR/TE = 4.50/1.82 msec, flip angle = 12 degrees, number of signal average = 1, matrix size = 512 × 512, FOV = 32 cm, and slice thickness = 1.5 mm. The imaging resolution (voxel size) was 0.6 × 0.6 × 1.5 mm. The segmentation of the fibroglandular tissue and fat was done on the pre-contrast images. The segmentation of the tumor was done on the subtraction images obtained by subtracting the pre-contrast images from the first frame of the post-contrast images acquired at 90 s after injection of Gd contrast agent.

2.3. Breast and fibroglandular tissue segmentation on MRI

We used a fully automatic template-based segmentation method to segment the breast and the fibroglandular tissue on MRI. Detailed procedures were described in Lin et al. [19, 20]. The segmentation of the breast was done by using a chest model with three body landmarks: the thoracic spine and the lateral margins of the bilateral pectoralis muscles. This chest template was coregistered to each subject's chest region to obtain a subject-specific chest model, and the three mapped landmarks were used to perform the initial V-shape cut to define the lateral boundaries [19]. The second step was to identify the chest wall muscle for further exclusion, by using edge detection algorithm and the Bezier curve fitting. The third step was to exclude the nipple and the skin using Bezier splines and dynamic search, detailed algorithms described in [20]. The left and right breasts were separated based on sternum. Within the segmented breast, the bias-field correction and k-means algorithm was applied to perform the segmentation of fibroglandular and fatty tissues.

2.4. Segmentation of the tumor

The tumor was segmented on the subtracted images using a fuzzy c-means (FCM) clustering based algorithm [21]. A square ROI selection was placed on maximum intensity projection map to indicate the location. The tumor within the selected ROI was enhanced using an unsharp filter [22] with a 5 by 5 kernel constructed using the inverse of the two-dimensional Laplacian filter [22]. FCM algorithm was applied to obtain the membership map of all voxels indicating the likelihood of each voxel belonging to the tumor or the non-tumor cluster. The weighting component on each fuzzy membership is chosen as 2, whereas the stopping criteria is the absolute change in objective function in consecutive iterations less than a pre-specified number 10^5 [23], and then the tumor membership map was binarized with the selected threshold to separate tumor from non-tumor voxels.

2.5. Evaluation of the tumor-fat interface

After obtaining the tumor mask, 2D connected-component labeling [24] was applied to remove the scattered voxels not connecting to the main body of lesion, and then the edge detection method [22] was utilized to obtain the boundary of the tumor mask. To evaluate the tumor-fat interface, both two dimensional (2D) and three dimensional (3D) analyses were performed. For the 2D analysis, the slice containing the largest tumor area among all

Author Manuscript Author Manuscript Author Manuscript Author Manuscript

the slices was selected. The pixels on the tumor boundary were identified, and for each pixel whether it was abutting to fat and fibroglandular tissue was determined. Three case examples are shown in Figs. 1–3. For the 3D analysis, the same analysis was performed for the tumor boundary pixels on all slices containing the tumor. The percentage was calculated as the ratio of the number of pixels abutting to fat to the total number of pixels.

2.6. Evaluation of the peritumoral fat

To analyze the peritumoral fatty tissue, three shells (SH1, SH2, SH3) surrounding the convex hall of the 3D tumor were defined, as demonstrated in Figs. 1–3. SH1 was defined as the shell between 150% volumetric expansion of the tumor convex hall subtracting the tumor convex hall (150%–100%); SH2 was (200%–150%); and SH3 was (250%–200%). In each shell the volumetric percentage of the peritumoral fatty tissue was calculated by dividing the fat volume to the shell volume.

2.7. Statistical analysis

A total of 5 parameters were measured: the 2D and 3D tumor-fat interface percentage and volumetric percentage of the peritumoral fatty tissue in the three shells. The distribution of each parameter, including the range, median, mean and standard deviation was reported. Two-tailed *t*-test was applied to evaluate the between-group difference. Person correlation was used to test the association between two continuous variables. A chi-square test was used to test whether the proportion of case numbers separated based on a cutoff value was significantly different between different tumor subtypes.

3. Results

3.1. Tumor-fat interface percentage

In all 102 tumors, the mean tumor-fat interface percentage was 39.7 ± 20.9% (median 38.4%, range, 0.5% – 85.1%) for 2D analysis performed on the tumor slice of the largest diameter, and 70.2 ± 18.9% (median 75.7%, range 15.3%–99.1%) for the 3D analysis performed on all tumor slices. The 3D measurement was significantly higher than the 2D measurement ($p < 0.001$), but they were highly correlated by using Pearson correlation ($r = 0.82$). There was no correlation between the tumor-fat interface percentage and tumor volume ($r = 0.18$ for 2D, and $r = 0.29$ for 3D). The results in each of the three molecular subtypes are shown in Table 1. In the TN group, the tumor-fat interface percentage was 43 ± 20% and 78 ± 12% using 2D and 3D measurement, the highest among the three subtypes but not significantly different ($p > 0.05$). In each molecular subtype, the number of cases was further separated into four groups by using the tumor-fat interface percentage of < 25%, 25–50%, 50–75%, and > 75%, and the results are shown in Table 2. No cut-off value could be used to significantly separate two tumor subtypes. For example, if using 2D tumor-fat interface percentage of > 50% as the cut off value, the proportion in HER2 positive group (19/46 = 41%) was higher than in HER2 negative groups (14/56 = 25%), but not significant ($p = 0.09$).

Author Manuscript Author Manuscript Author Manuscript Author Manuscript

3.2. Peritumoral volumetric fat percentage

The volumetric fat percentage of the whole cohort (N = 102) in SH1, SH2, and SH3 were 65.4 ± 18.0%, 73.1 ± 16.4%, and 76.7 ± 15.3%, respectively. The results in three molecular subtypes are shown in Table 1. The fat percentage increases from SH1 to SH2 to SH3, all significant, indicating that the tissue becomes fattier and fattier away from the tumor. Since the fibroglandular tissue density is higher in the nipple than the peripheral region of a breast, this finding is highly anticipated. Another possibility is that the malignant cells may take energy from the nearby fatty area as fuel for their tumor growth. The volumetric fat percentage in SH2 and SH3 in the TN group is 82 ± 7% and 85 ± 7%, which was significantly higher compared to the non-TN (two other) tumor subtypes (p = 0.038 and p = 0.047 respectively). The significance remained after controlling for the whole breast fat percentage.

4. Discussion

The motivation to conduct this study was based on the biological fact that peritumoral tissue plays an important role in tumorigenesis [25]. The high spatial resolution of 3D MRI provided a good tissue contrast between fatty and fibroglandular tissue as well as the strong contrast enhancement of the tumor, made the tissue segmentation possible for developing the quantitative analysis method. In this study we measured 5 parameters, including the tumor-fat interface percentage on a 2D slice with the largest tumor area and on the 3D tumor from all slices, as well as the peritumoral volumetric fat percentage in three shells surrounding the tumor.

Only a few studies investigated the association of breast fatty tissue with tumor characteristics using qualitative [12, 13, 26] or quantitative analysis approaches [13]. In an early study using mammograms in women younger than 50 years of age, it was noted that most mammographically detected cancers (63 of 86 = 73%) were located at the periphery of the parenchymal cone, which was defined by a 1-cm wide zone beneath the subcutaneous or retromammary fat [26]. In this study we also investigated how many tumors were located at the periphery of the parenchymal cone using MRI. We selected the slice with the largest tumor area in each patient. On this slice, the convex hull of the fibroglandular tissue mask was extracted.

We then calculated a 1-cm isotropic area expansion, and a 1-cm isotropic area shrinkage, around the convex hull. Then a shell was obtained by subtracting the shrinkage area from the expansion area. If a tumor contacted with the shell, the location of the tumor was considered as at the periphery of the parenchymal cone. With this definition we noted that 61 out of 102 patients (59.8%) had tumor growing from this location. In an MRI study of 294 patients with biopsy-proven invasive breast, the location of breast tumor in relation to the fatty tissue was visually assessed by comparing the contrast-enhanced MRI images and the corresponding T1-weighted pre-contrast images [12], and the results showed a very high percentage of tumor abutting fatty tissue (29½94, 98.9%). Another large series study of 881 women evaluated the location of breast lesions with respect to the fat-gland interface in MR imaging using both qualitative and quantitative approaches [13]. For qualitative analyses, the radiologists visually graded the breast lesions based on their spatial relationships with the

Author Manuscript Author Manuscript Author Manuscript Author Manuscript

fat-gland interface in the breast using five categories (2 = within the gland; 1 = near the fat-gland interface, gland side; 0 = fat-gland interface; −1 = near the fat-gland interface, fat side; and −2 = within the fat). For quantitative approaches, the radiologist measured the shortest distance between the center of the lesion and the fat-gland interface on the sagittal or axial image. A positive value was assigned when the tumor center was in the gland tissue, and a negative value was assigned when the tumor center was in the fatty tissue. It was found that most breast lesions were located in or near the fatty tissue interface either by qualitative (89.7%) or quantitative (90.0%) analyses [13]. All these studies support that local breast fatty tissue is biologically important in development of breast cancer.

Our study applied a morphological segmentation method to quantitatively measure the tumor-fat interface percentage using 2D and 3D approaches. To achieve the goal, sophisticated breast and fibroglandular tissue segmentation methods, as well as the tumor segmentation methods, were needed. The segmentation methods used in this study were well-developed and have been used in many previous publications. Our results noted the average of tumor-fat interface percentage using 2D and 3D measurement was 40% and 70% respectively, and measurements from the both methods were highly correlated ($r = 0.82$). The higher value in 3D analysis was anticipated, since the outer layer of the breast was more likely to be fat. We also noted that both 2D and 3D results did not show significant difference between TN and non-TN tumors, or between HER2 positive and HER2 negative tumors.

We further measured the percentage of peritumoral fatty tissue in different shells surrounding the tumor. The idea of dividing the peritumoral tissue into several layers with various distances from the center of the tumor has been conducted in several previous studies [14, 16, 18, 27, 28]. This approach allows for examining the tissue changes from the proximity of the tumor to the far field. There were two general methods used in the literature, one with various distances of radius from the tumor margin [16, 18, 27], and the other with isotropic volumetric expansion around the tumor [14]. Our study adopted the second approach. We determined to select 150%, 200% and 250% to define the peritumoral shells. For the first shell near the tumor (SH1), if a smaller ratio was used, such as 125%, it might lead to thin shells which sometimes could not be correctly processed, especially in small tumor lesions, to extract the tissue characteristics within the shells. If a larger ratio, such as 300%, was utilized, large amount of normal fibrograndular tissue might be included and the tissue heterogeneity inside the shells would be too substantial, which was meaningless for this study. With this approach, the thickness of the three peritumoral shells thus was variable patient to patient according to their tumor size. For example, if a patient had a tumor measured 2 cm in one-dimension, the thickness for each of the three peritumoral shells was 0.5 cm. If a patient had a 5 cm tumor, the thickness for each of the three peritumoral shells was 1.25 cm.

In a study to characterize breast cancer and adjacent peritumoral stroma using high-resolution diffusion-weighted imaging, three peritumoral shells (2–6 pixels, 14–18 pixels, and 26–30 pixels outside the tumor ROI) were defined [18]. In a study using multi-parametric MRI to evaluate the prognostic impact of peritumoral fat in early stage breast cancer, the shell was constructed by subtracting the tumor volume from a 1-cm isotropic

Author Manuscript Author Manuscript Author Manuscript Author Manuscript

volumetric expansion around it [14]. Overall, the peritumoral tissue is a loosely defined term, as there is no consensus about how far away from the tumor or how wide the zone should be. Our results showed that the volumetric fat percentage in SH2 and SH3 in the TN group was significantly higher than in non-TN tumor subtypes ($p = 0.038$ and $p = 0.047$ respectively). The results remained significant after controlling for the whole breast fat percentage.

Although the findings of the higher volumetric fat percentage in the peritumoral shells in TN tumors were preliminary, pending further clarification, there may be potential clinical relevance which can improve patient management. TN subtype was very aggressive and found to have a statistically significant association with an increased risk of residual tumor and locoregional recurrence, regardless that margin status, size, and multifocality were similar among the TN and luminal subtypes [29]. Studies had also found the association of adiposity with cancer incidence, morbidity and mortality [14]. The mechanisms by which peritumoral human adipose tissue contributes to TN breast cancer cell invasiveness and dissemination has been studied [29]. The study reported that cancer cell growth and/or metastasis predominantly occur in adipocyte-rich microenvironment [30]. In nodal positive patients, the peritumoral fat ratio was found to correlate with the axillary lymph node status [14]. A recent study [31] further showed that TN tumors may depend on fat as fuel for the tumor growth; an unusual abundance of fatty acid oxidation metabolites was noted, indicating that TN cancer cells may be oxidizing fat to satisfy their energy needs. With all these findings, it may be interesting to develop new therapeutic strategies to target fat oxidation to control the growth of TN tumor, or the findings may help the breast surgeons to plan the surgical resection margin to reduce the recurrence rate.

This study had limitations. The total case number was small, especially the TN subtype. Thus all the findings in this study were very preliminary and no definite conclusion could be drawn yet. Also, breast volume, the tumor location, and tumor size may affect the definition of peritumoral shells. For some patients with large tumor volume compared with the breast volume, the difference among the peritumoral shells became small. If a patient had a tumor close to the skin, the assignment of the peritumoral shells, especially for SH2 and SH3, might be limited by the breast boundary, thus tissue information surrounding the tumor in these shells could not be completely evaluated.

In conclusion, in this study a three-dimensional (3D) morphological analytic method was developed to quantitatively measure the tumor-fat interface percentage and the volumetric fat percentage in different peritumoral shells surrounding the tumor. This method was relying on the precise tissue segmentation, which was only feasible based on the high tissue contrast between fibroglandular and fatty tissue on MRI, as well as the strong contrast enhancement of the tumor for identifying the tumor boundary on MRI. The results showed that the peri-tumor fat content was the highest in the most aggressive TN tumors compared to other subtypes. But due to the small case number, the significance of the findings was not confirmed yet and should be validated in a larger dataset. The developed quantitative analysis method may be applied to further investigate the clinical significance of the peritumoral fat in the development and prognosis of breast cancer.

Author Manuscript Author Manuscript Author Manuscript Author Manuscript

Acknowledgement

This work was supported in part by NIH/NCI Grant No. R01 CA127927, R21 CA170955, R21 CA208938, and R03 CA136071.

References

[1]. Mohammed ZM, McMillan DC, Edwards J, Mallon E, Doughty JC, Orange C, et al. The relationship between lymphovascular invasion and angiogenesis, hormone receptors, cell proliferation and survival in patients with primary operable invasive ductal breast cancer. BMC Clin Pathol 2013;13:31. [PubMed: 24274633]

[2]. Lee AK, DeLellis RA, Silverman ML, Heatley GJ, Wolfe HJ. Prognostic significance of peritumoral lymphatic and blood vessel invasion in nodenegative carcinoma of the breast. J Clin Oncol 1990;8:1457–65. [PubMed: 2202788]

[3]. Uematsu T Focal breast edema associated with malignancy on T2-weighted images of breast MRI: peritumoral edema, prepectoral edema, and subcutaneous edema. Breast Cancer 2015 1;22(1): 66–70. [PubMed: 25336185]

[4]. Chai H, Brown RE. Field effect in cancer - an update. Ann Clin Lab Sci 2009;39:331–7. [PubMed: 19880759]

[5]. Heaphy CM, Griffith JK, Bisoffi M. Mammary field cancerization: molecular evidence and clinical importance. Breast Cancer Res Treat 2009;118:229–39. [PubMed: 19685287]

[6]. Lapeire L, Denys H, Cocquyt V, De Wever O. When fat becomes an ally of the enemy: adipose tissue as collaborator in human breast cancer. Horm Mol Biol Clin Invest 2015 7;23(1):21–38.

[7]. Tahergorabi Z, Khazaei M, Moodi M, Chamani E. From obesity to cancer: a review on proposed mechanisms. Cell Biochem Funct 2016 12;34(8):533–45. [PubMed: 27859423]

[8]. Schäffler A Mechanisms of disease: adipokines and breast cancer - endocrine and paracrine mechanisms that connect adiposity and breast cancer. Nat Clin Pract Endocrinol Metab 2007;3(4):345–54. [PubMed: 17377617]

[9]. Beer AE. Adipose tissue, a neglected factor in aetiology of breast cancer? Lancet 1978;2:96.

[10]. Wang F, Gao S, Chen F, Fu Z, Yin H, Lu X, et al. Mammary fat of breast cancer: gene expression profiling and functional characterization. PLoS One 2014 10 7;9(10):e109742. [PubMed: 25291184]

[11]. Freed M, Storey P, Lewin AA, Babb J, Moccaldi M, Moy L, et al. Evaluation of breast lipid composition in patients with benign tissue and cancer by using multiple gradient-echo MR imaging. Radiology 2016 10;281(1):43–53. [PubMed: 27266558]

[12]. Zhu W, Harvey S, Macura KJ, Euhus DM, Artemov D. Invasive breast cancer preferably and predominantly occurs at the interface between fibroglandular and adipose tissue. Clin Breast Cancer 2017 2;17(1):e11–8. [PubMed: 27568102]

[13]. Kim WH, Li M, Han W, Ryu HS, Moon WK. The spatial relationship of malignant and benign breast lesions with respect to the fat-gland interface on magnetic resonance imaging. Sci Rep 2016 12 14;6:39085. [PubMed: 27966625]

[14]. Obeid JP, Stoyanova R, Kwon D, Patel M, Padgett K, Slingerland J, et al. Multiparametric evaluation of preoperative MRI in early stage breast cancer: prognostic impact of peri-tumoral fat. Clin Transl Oncol 2017 2;19(2):211–8. [PubMed: 27364695]

[15]. Wang YY, Lehuédé C, Laurent V, Dirat B, Dauvillier S, Bochet L, et al. Adipose tissue and breast epithelial cells: a dangerous dynamic duo in breast cancer. Cancer Lett 2012 11 28;324(2):142–51. [PubMed: 22643115]

[16]. Braman NM, Etesami M, Prasanna P, Dubchuk C, Gilmore H, Tiwari P, et al. Intratumoral and peritumoral radiomics for the pretreatment prediction of pathological complete response to neoadjuvant chemotherapy based on breast DCE-MRI. Breast Cancer Res 2017 5 18;19(1):57. [PubMed: 28521821]

[17]. Mori N, Mugikura S, Takasawa C, Miyashita M, Shimauchi A, Ota H, et al. Peritumoral apparent diffusion coefficients for prediction of lymphovascular invasion in clinically node-negative invasive breast cancer. Eur Radiol 2016 2;26(2):331–9. [PubMed: 26024846]

Author Manuscript Author Manuscript Author Manuscript Author Manuscript

[18]. Shin HJ, Park JY, Shin KC, Kim HH, Cha JH, Chae EY, et al. Characterization of tumor and adjacent peritumoral stroma in patients with breast cancer using high-resolution diffusion-weighted imaging: correlation with pathologic biomarkers. Eur J Radiol 2016 5;85(5):1004–11. [PubMed: 27130063]

[19]. Nie K, Chen JH, Chan S, Chau MK, Yu HJ, Bahri S, et al. Development of a quantitative method for analysis of breast density based on three-dimensional breast MRI. Med Phys 2008 12;35(12): 5253–62. [PubMed: 19175084]

[20]. Lin M, Chen JH, Wang X, Chan S, Chen S, Su MY. Template-based automatic breast segmentation on MRI by excluding the chest region. Med Phys 2013 12;40(12):122301. [PubMed: 24320532]

[21]. Nie K, Chen JH, Yu HJ, Chu Y, Nalcioglu O, Su MY. Quantitative analysis of lesion morphology and texture features for diagnostic prediction in breast MRI. Acad Radiol 2008 12;15(12):1513–25. [PubMed: 19000868]

[22]. Gonzalez Rafael C, Woods Richard E, Eddins Steven L. Digital image processing using MATLAB Pearson Education; 2004 (ISBN 978-81-7758-898-9).

[23]. Bezdec JC. Pattern recognition with fuzzy objective function algorithms New York: Plenum Press; 1981.

[24]. Haralick Robert M, Shapiro Linda G. Computer and Robot Vision Vol. I Addison-Wesley; 1992 p. 28–48.

[25]. Polyak K, Kalluri R. The role of the microenvironment in mammary gland development and cancer. Cold Spring Harb Perspect Biol 2010 11;2(11):a003244. [PubMed: 20591988]

[26]. Stacey-Clear A, McCarthy KA, Hall DA, Pile-Spellman E, White G, Hulka CA, et al. Mammographically detected breast cancer: location in women under 50 years old. Radiology 1993;186:677–80. [PubMed: 8381550]

[27]. Jones EF, Sinha SP, Newitt DC, Klifa C, Kornak J, Park CC, et al. MRI enhancement in stromal tissue surrounding breast tumors: association with recurrence free survival following neoadjuvant chemotherapy. PLoS One 2013 5 7;8(5):e61969. [PubMed: 23667451]

[28]. McLaughlin RL, Newitt DC, Wilmes LJ, Jones EF, Wisner DJ, Kornak J, et al. High resolution in vivo characterization of apparent diffusion coefficient at the tumor-stromal boundary of breast carcinomas: a pilot study to assess treatment response using proximity-dependent diffusion-weighted imaging. J Magn Reson Imaging 2014 5;39(5):1308–13. [PubMed: 24719242]

[29]. Sioshansi S, Ehdaivand S, Cramer C, Lomme MM, Price LL, Wazer DE. Triple negative breast cancer is associated with an increased risk of residual invasive carcinoma after lumpectomy. Cancer 2012 8 15;118(16):3893–8. [PubMed: 22864932]

[30]. D'Esposito V, Liguoro D, Ambrosio MR, Collina F, Cantile M, Spinelli R, et al. Adipose microenvironment promotes triple negative breast cancer cell invasiveness and dissemination by producing CCL5. Oncotarget 2016 4 26;7(17):24495–509. [PubMed: 27027351]

[31]. Camarda R, Zhou AY, Kohnz RA, Balakrishnan S, Mahieu C, Anderton B, et al. Inhibition of fatty acid oxidation as a therapy for MYC-overexpressing triple-negative breast cancer. Nat Med 2016 4;22(4):427–32. [PubMed: 26950360]

Author Manuscript Author Manuscript Author Manuscript Author Manuscript

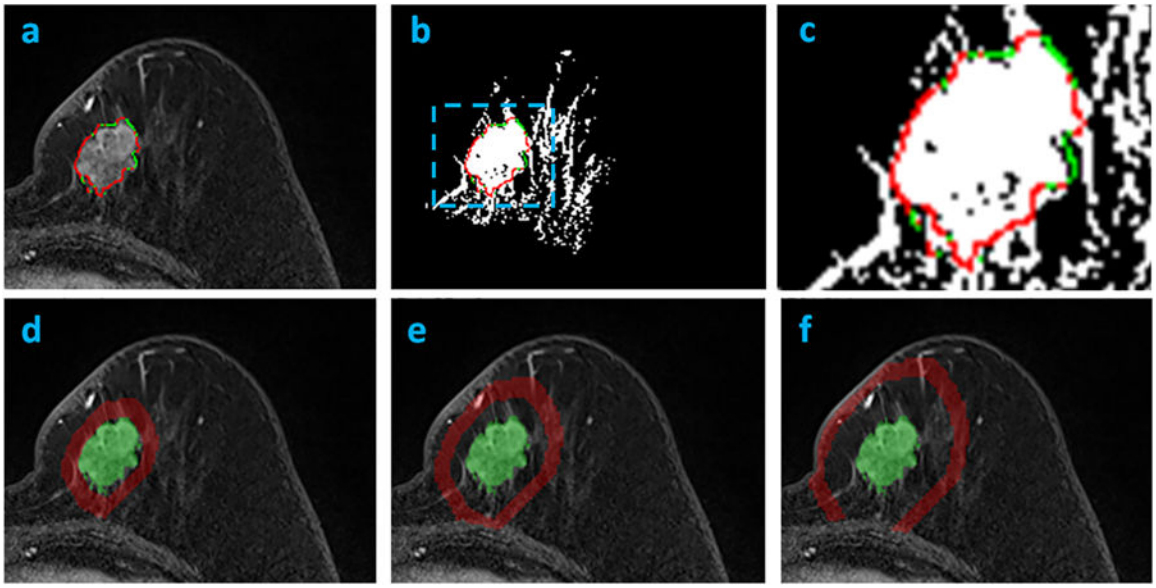

Fig. 1.

A 75-years-old woman with a triple negative TN cancer in the left breast. (a) Contrast-enhanced subtraction image; (b) Corresponding fibroglandular tissue mask; (c) Zoom-in image to show the lesion boundary. The red and green contours represent pixels interfacing with fibroglandular tissue and fat, respectively. (d) SH1 defined as the shell between (150%–100%) expansion of the tumor convex hall; (e) SH2 (200%–150%); and (f) SH3 (250%–200%). The whole breast fat percentage is 94%. The peri-tumor interface fat percentage is 35%, and the volumetric fat percentage in SH1, SH2, and SH3 is 72%, 84%, and 87%, respectively. (For interpretation of the references to color in this figure legend, the reader is referred to the web version of this article.)

Author Manuscript Author Manuscript Author Manuscript Author Manuscript

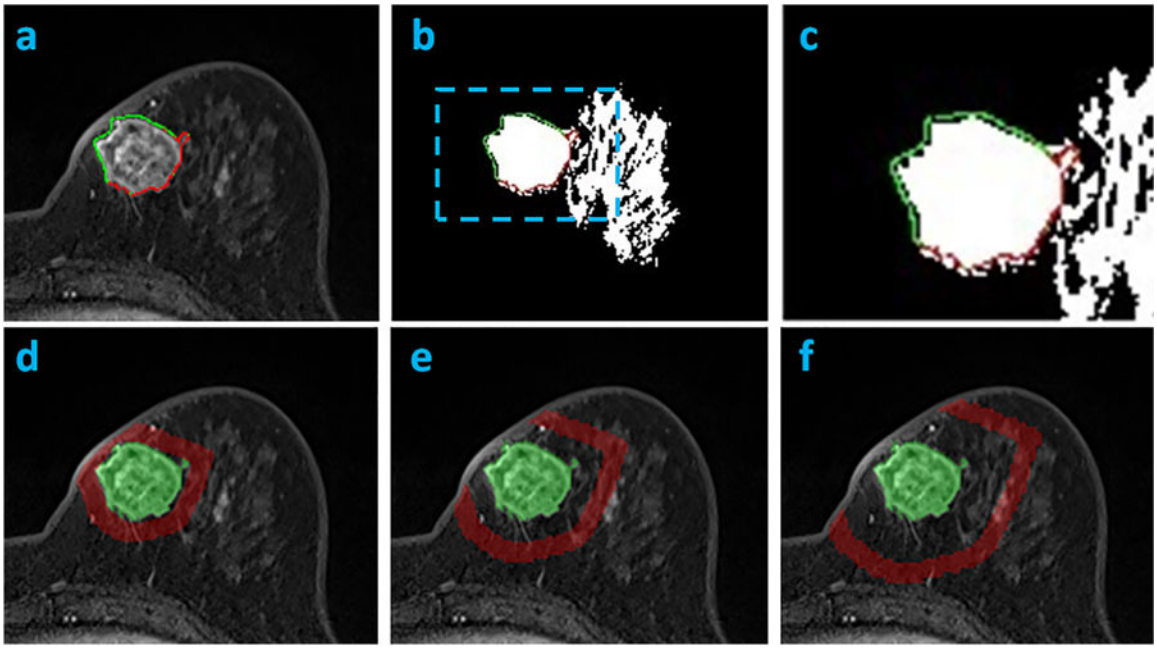

Fig. 2.

A 58-years-old woman with a HR(−)HER2(+) cancer in the left breast. (a) Contrast-enhanced subtraction image; (b) Corresponding fibroglandular tissue mask; (c) Zoom-in image to show the lesion boundary. The red and green contours represent pixels interfacing with fibroglandular tissue and fat, respectively. (d) SH1 defined as the shell between (150%–100%) expansion of the tumor convex hall; (e) SH2 (200%–150%); and (f) SH3 (250%–200%). The whole breast fat percentage is 86%. The peri-tumor interface fat percentage is 52%, and the volumetric fat percentage in SH1, SH2, and SH3 is 79%, 75%, and 71%, respectively. (For interpretation of the references to color in this figure legend, the reader is referred to the web version of this article.)

Author Manuscript Author Manuscript Author Manuscript Author Manuscript

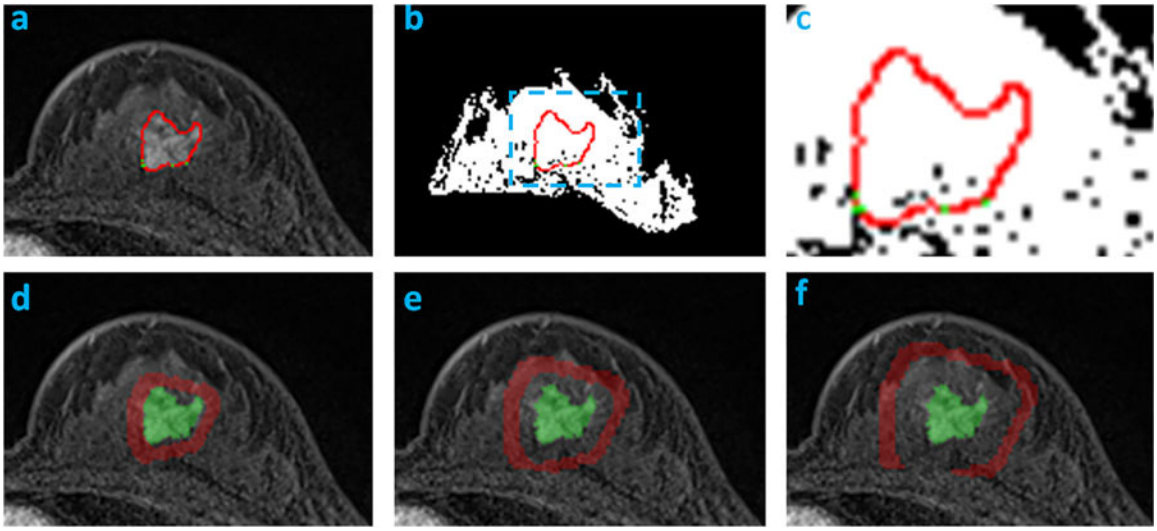

Fig. 3.

A 58-years-old woman with a HR(+) cancer in the left breast. (a) Contrast-enhanced subtraction image; (b) Corresponding fibroglandular tissue mask; (c) Zoom-in image to show the lesion boundary. The red and green contours represent pixels interfacing with fibroglandular tissue and fat, respectively. (d) SH1 defined as the shell between (150%–100%) expansion of the tumor convex hall; (e) SH2 (200%–150%); and (f) SH3 (250%–200%). The whole breast fat percentage is 58%. The peri-tumor interface fat percentage is 4%, and the volumetric fat percentage in SH1, SH2, and SH3 is 17%, 39%, and 54%, respectively. (For interpretation of the references to color in this figure legend, the reader is referred to the web version of this article.)

Author Manuscript

Author Manuscript

Author Manuscript

Author Manuscript

Table 1

The mean ± standard deviation of the tumor-fat interface percentage and peritumoral volumetric fat percentage in three molecular subtypes.

	HER2(+) ***N*** **= 46**	**HER2(−)HR(+)** **N = 46**	**TN** ***N*** **= 10**
2D Tumor-Fat Interface Percentage	43 ± 21%	36 ± 21%	43 ± 20%
3D Tumor-Fat Interface Percentage	72 ± 18%	67 ± 21%	78 ± 12%
Shell-1 (SH1) Volumetric Fat Percentage	65 ± 18%	58 ± 21%	67 ± 12%
Shell-2 (SH2) Volumetric Fat Percentage	75 ± 14%	69 ± 17%	82 ± 7%*
Shell-3 (SH3) Volumetric Fat Percentage	78 ± 14%	73 ± 16%	85 ± 7%*

*Denotes significant difference ($p < 0.05$) between TN and non-TN tumors.

Author Manuscript

Author Manuscript

Author Manuscript

Author Manuscript

Table 2

Number of patients based on tumor-fat interface percentage of < 25%, 25–50%, 50–75%, > 75%.

	HER2(+) ***N*** **= 46**	**HER2(−)HR(+)** **N = 46**	**TN** ***N*** **= 10**
2D			
Tumor-Fat Interface Percentage < 25%	11 (24%)	15 (33%)	1 (10%)
Tumor-Fat Interface Percentage 25–50%	16 (35%)	21 (46%)	5 (50%)
Tumor-Fat Interface Percentage 50–75%	17 (37%)	8 (17%)	3 (30%)
Tumor-Fat Interface Percentage > 75%	2 (4%)	2 (4%)	1 (10%)
3D			
Tumor-Fat Interface Percentage < 25%	1 (2%)	2 (4%)	0
Tumor-Fat Interface Percentage 25–50%	4 (9%)	6 (13%)	0
Tumor-Fat Interface Percentage 50–75%	17 (37%)	16 (35%)	3 (30%)
Tumor-Fat Interface Percentage > 75%	24 (52%)	22 (48%)	7 (70%)